Catalysis Science & Technology

ROYAL SOCIETY OF CHEMISTRY

PAPER

View Article Online
View Journal | View Issue

Cite this: *Catal. Sci. Technol.*, 2022, **12**, 1850

Ligand assisted hydrogenation of levulinic acid on Pt(111) from first principles calculations†

Lars Gell and Karoliina Honkala *

In this study, we investigate the hydrogenation reaction of levulinic acid to 4-hydroxypentanoic acid on ligand-modified Pt(111) using DFT. Modifying nanoparticle surfaces with ligands can have beneficial effects on the desired reaction such as improved selectivity or lower activation energies. The N^3,N^3-dimethyl-N^2-(quinolin-2-yl)propane-1,2-diamine (AQ) ligand was selected to modify the surface, since it combines good surface adsorption properties with functional groups that can influence the reaction. The adsorption geometry of the AQ ligand was studied as well as the co-adsorption of a second AQ ligand for the possibility of self-assembly. We found that dissociated hydrogen from the Pt(111) surface can protonate the AQ ligand and discuss the role this plays on the mechanism of the hydrogenation reaction of levulinic acid (LA). By comparing the ligand-modified Pt(111) surface to the bare Pt(111) surface we show that the reaction changes from a step-wise to a concerted mechanism due to the influence of the ligand molecule. This demonstrates the effect that ligand-modified surfaces can have on catalyzing reactions and shows that desired reactions can be achieved by tuning the reaction environment.

Received 10th November 2021,
Accepted 20th January 2022

DOI: 10.1039/d1cy02048j

rsc.li/catalysis

1 Introduction

Enantiopure compounds, ranging from fundamental synthetic building blocks like amino acids or epoxides to commercial end products such as drugs and food additives,[1,2] are extensively used in the chemical and pharmaceutical industries. This creates a demand for large scale enantioselective production processes. Traditionally, enantioselective syntheses are carried out using asymmetric homogeneous catalysts made of chiral transition metal complexes.[3] These molecular catalysts mostly feature one central metal atom bonding with multiple, often different, ligands. The ligand molecules' influence on the overall properties of a transition metal complex is significant, and therefore their role in the activity and selectivity in asymmetric homogeneous catalysis as well as in the stability of the catalyst has been extensively studied.[4–7] Metal complex-based catalysis, however, suffers from limitations such as low operation temperatures and difficulties in separating the products from the catalysts.[4,8] Metal nanoparticles can circumvent these shortcomings.[9–14] Due to their unique properties, such as high surface-to-volume ratio and a large number of low coordinated sites, metal nanoparticles provide high stability combined with the possibility of high reactivity.[15,16] Unfortunately, this often comes at the expense of high enantioselectivity due to the multiple reaction sites which can lead to different reaction mechanisms and, consequently, the formation of different products. Introducing ligands on metal nanoparticles is one way to improve the enantioselectivity.[17,18] Adsorbed ligands can be used to block certain reaction sites or mechanisms, tune the steric and electronic interactions with a reactant molecule, and modify the chemical properties of the surface, such as hydrophilicity, acidity, and chirality.[19–21] Ultimately, this will lead to highly specific reaction environments, similar to those of enzymes, that are tailored towards the desired product.

Ligand design is crucial in creating self-assembled enzyme-like reactant environments to control reaction mechanisms and achieve optimal enantioselectivity. A large variety of ligand molecules such as N-heterocyclic carbenes,[22,23] secondary phosphine-oxides,[24] thiols,[25] amino acids,[26] and aminidates[27] can be used to decorate metal nanoparticles.[19,28] Many ligand-modified late transition metal nanoparticles have shown catalytic activity[19] towards reactions such as the hydrogenation of organic acids, ketones and alcohols,[29] the reduction of CO_2,[30] and the oxidation of C–C-double bonds.[31] For hydrogenation reactions on Pt, cinchona alkaloid ligands have shown promising experimental results[9,11,32–34] such as high enantioselectivity in multiple ketone reduction reactions.[35] According to density functional theory (DFT) calculations, quinoline-type ligands show strong binding energies on Pt(111) surfaces, especially

Department of Chemistry, Nanoscience Center, University of Jyväskylä, P.O. Box 35, FI-40014 Jyväskylä, Finland. E-mail: karoliina.honkala@jyu.fi

† Electronic supplementary information (ESI) available. See DOI: 10.1039/d1cy02048j

when they are co-adsorbed with hydrogen or oxygen, making them stable under moderate reaction conditions.[36]

One key application of asymmetric catalysis is the transformation of biomass into value added products through hydrogenation reactions like the reduction of levulinic acid (LA) to γ-valerolactone (GVL).[37] LA is a versatile platform chemical that can be obtained on an industrial scale from biomass which is often a byproduct of agricultural production, *e.g.*, wheat straw.[38,39] GVL is another important platform chemical for fuel and fine chemical production.[37,40,41] Several experimental and computational studies have shown that the hydrogenation of LA can occur *via* homogeneous as well as heterogeneous catalysis.[42–47] The homogeneously catalyzed reduction of LA to GVL can be achieved using various transition metal complexes.[44,46,48] Previous DFT studies have shown low activation energies (<0.3 eV) for this transition.[44,46] Heterogeneous reduction of LA has been addressed on bare metals,[42] metal alloys[41] and metal oxides.[49] Ru-Catalyzed LA reduction can follow two different mechanisms: the alkoxy mechanism and the hydroxy mechanism. In the alkoxy mechanism, hydrogen initially forms a bond with the carbonyl carbon atom followed by a second hydrogen bonding with the carbonyl oxygen atom. The hydrogen addition steps are reversed in the hydroxy mechanism.[42] The transformation to 4-hydroxypentanoic acid (4-HPA) is endothermic by 0.81 eV, and that to GVL is exothermic by 0.05 eV.[42] In general, for the transformation to GVL, the alkoxy mechanism is favoured with an activation barrier of 0.5 eV whereas the hydroxy mechanism shows an activation barrier of more than 1 eV.[42] Previous calculations have shown that solvents affect the hydrogenation of LA. Solvents with higher polarity than methanol, such as water, create a more favourable reaction environment, thereby lowering the rate determining barrier by 0.1 eV.[47] Lower reaction rates for the reduction of LA have been experimentally observed on Pt surfaces[45,50] compared to those of other transition metals (*e.g.*, Ru and Pd), suggesting higher selectivity.[51,52]

In the present study, we address the reduction of LA on a ligand-modified Pt(111) surface. We choose a 2-amino-quinoline derivative to modify the surface because it binds sufficiently strongly to Pt(111) and allows intermolecular hydrogen bonding as well as ligand–reactant interaction. The self-assembly of these ligands and the influence of their structure on the reduction of LA are discussed. Furthermore, we demonstrate how the introduction of an amino-quinoline derivative can modify the reaction mechanism, thereby opening the possibility for higher enantioselectivity.

2 Computational details

2.1 DFT

We used density-functional theory (DFT) with a projector augmented wave method (PAW)[53] as implemented in the real-space grid code-package GPAW.[54–56] In the finite difference (FD) mode, the PAW setup was defined for the atomic valence of $Pt(5p^6 6s^1 5d^9)$, $O(2s^2 2p^4)$ $N(2s^2 2p^3)$, $C(2s^2 2p^2)$, and $H(1s^1)$, with scalar-relativistic effects included for Pt. Total energy calculations and structure optimizations were done using the BEEF-vdW[57] exchange correlation functional together with a geometry convergence criterion of 0.05 eV Å^{-1} for the residual forces acting on atoms. The convergence criteria for each SCF cycle are: maximum change in energy = 0.0005 eV per valence electron, maximum change in density (integrated absolute value of density change) = 1.0×10^{-4} electrons per valence electron and maximum changes to the eigenstates = 4.0×10^{-8} eV^2 per valence electron. The Pt(111) surface was modelled as a 4-layer thick 7 × 7 2D slab cut from Pt bulk with a lattice constant of 4.02 Å. We used a 19.9 × 19.9 × 25.0 Å^3 unit cell with 96 × 96 × 128 grid points and periodic boundary conditions in the surface plane. The two topmost layers were relaxed, and the remaining bottom layers were fixed into their bulk positions. The calculations were carried out with a single Γ-point. The adsorption geometries of AQ were screened using the localized atomic orbitals (LCAO)[58] method with single zeta basis sets on all the atoms. Transition states were identified using the climbing image NEB method[59,60] and confirmed through vibrational frequency analysis along the reaction coordinate using the Frederiksen method.[61] The imaginary frequencies for transition states are given in Table S1.† The calculations were performed on a 3-layer thick slab to reduce the computational costs. The Bader method[62] was employed to evaluate individual atomic partial charges. The adsorption energies were calculated according to the equation

$$E_{\mathrm{adsorb}} = E_{\mathrm{ads}} - (E_{\mathrm{surf}} + E_{\mathrm{gas}}) \quad (1)$$

where E_{ads} is the energy of the surface and the adsorbed molecule, E_{surface} is the energy for the bare surface, and E_{gas} represents the energy of the molecule in the gas phase.

2.2 Structural details

N^3,N^3-Dimethyl-N^2-(quinolin-2-yl)propane-1,2-diamine (AQ) (Fig. 1) was selected as a ligand to modify the Pt(111) surface. With this ligand selection, we aim to achieve three key elements: 1) strong binding to Pt(111) in order to ensure catalyst stability under reaction conditions. Based on the binding properties of cinchona alkaloids, we choose a quinoline double ring as the anchoring unit to ensure a

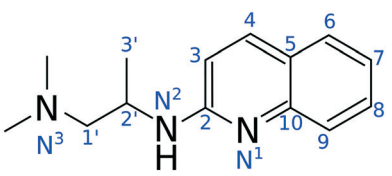

Fig. 1 The structure of the AQ ligand molecule, N^1,N^1-dimethyl-N^2-(quinolin-2-yl)propane-1,2-diamine, is shown, where the blue letters and numbers indicate the notation of individual atoms that will be referenced later.

strong ligand–surface interaction. 2) This ligand offers the possibility for attractive ligand–ligand and ligand–reactant interactions through intermolecular hydrogen bonds. These interactions have the possibility of creating self-assembled enzyme-like reaction environments. 3) A ligand may have a beneficial influence on the enantioselectivity of the desired reaction. Potential strategies to achieve this are the limitation of adsorption configurations for the reactant (lock and key principle), the modification of the reaction mechanism, and the kinetic discrimination of unwanted configurations. In the case of a single AQ ligand, more than 50 different adsorbed structures were screened at the LCAO level of theory, and 20 of them were further optimized using the FD method, while in the case of two co-adsorbed AQ ligands the number of structures was reduced to 20 and 11, respectively. On the bare Pt(111) surface, the reaction pathways were calculated for both levulinic acids with (LA1) and without (LA2) an internal hydrogen bond. Due to the higher computational costs, we focused on the reduction of LA2 in the case of the ligand modified surface.

3 Results and discussion

3.1 Binding of AQ onto Pt(111)

AQ configurations on the Pt(111) surface were divided into 3 classes according to certain structural features. Class A shows the N^3 atom at a greater distance from the surface than its neighbouring carbon atoms and the C2′–C3′ bond parallel to the surface. Class B is characterized by having the C3′ and the N^3 atoms closer to the surface than their neighbouring carbon atoms. In class C, the tertiary amine moiety is close to the surface as in class B, while the C2′–C3′ bond points away from the surface. The most energetically favoured configuration in each class is shown in Fig. 2. All classes bind to the Pt(111) surface through the quinoline moiety. Three energetically most favourable configurations from each class were selected and then relaxed at the FD level, as described above. The adsorption energy depends on the conformation of the AQ ligand, particularly the position of the quinoline moiety, as well as the adsorption site on Pt(111). In general, orientations in which the quinoline double ring system is not parallel to the Pt surface are energetically very unfavourable. In the most energetically favoured geometries, the quinoline rings are sitting over a rhomboid Pt_4 unit with ring–surface distances varying between 2.2 Å and 3.5 Å. These short distances, together with an exothermic adsorption energy of −1.22 eV per molecule, are a clear indication of chemisorption. The adsorption energy for AQ on Pt(111) is significantly more exothermic than that for cinchonidine (about −0.4 eV per molecule).[32–34,63] Short distances between the quinoline group and the surface are energetically favoured, while short distances between the N^3 nitrogen and the surface are energetically unfavoured (see Table 1, as well as Fig. S2†).

Table 1 Adsorption energies and selected distances for the AQ structures shown in Fig. 2

	E_{adsorb} (eV)	N^3–Pt dist. (Å)	Ring–Pt dist. (Å)
a)	−1.22	3.78	2.71
b)	−1.06	3.84	3.10
c)	−0.79	3.10	2.40

3.2 AQ co-adsorption

The co-adsorption of ligands is an important step towards a self-assembled layer which creates an enantioselective reaction environment. We therefore also explore the energetics and structural features of two co-adsorbed AQ molecules. In order to reduce the computation expense, only the three best conformers shown in Fig. 2 were considered and combined to investigate the different orientations of the two co-adsorbed AQ ligands (2AQ). The initial structures were generated by introducing the second AQ ligand into the unit cell and then translating and rotating it with respect to the initial AQ ligand while keeping similar AQ–surface distances as reported in Table 1. The three selected configurations shown in Fig. 3 highlight the effect of the alignment of class A ligands with respect to each other and the distance between them. As expected, given the higher adsorption energies for class B and class C molecules, combinations of these conformations are also less energetically favourable. In

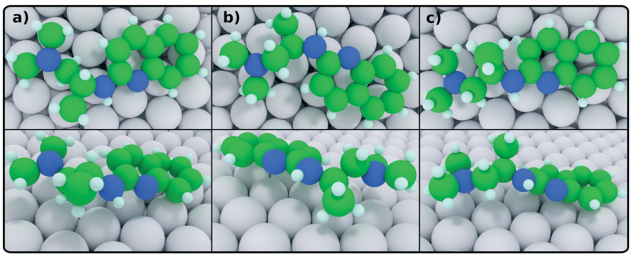

Fig. 2 The most energetically favoured structures from each class are shown. The corresponding relative energies are a) 0.00 eV for class A, b) 0.17 eV for class B, and c) 0.44 eV for class C, and the absolute energies and interatomic distances can be found in Table 1.

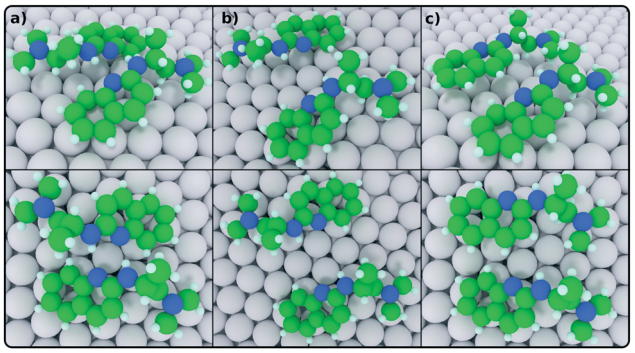

Fig. 3 The adsorption geometries of the three selected co-adsorption structures are shown. The corresponding energies are a) 0.00 eV (anti-parallel), b) 0.07 eV (separated), and c) 0.17 eV (parallel).

the lowest energy configuration, the AQ ligands are antiparallel to each other. This leads to the formation of two intermolecular hydrogen bonds between the secondary amine on one ligand and the quinoline nitrogen atom on the other ligand. As a result, the distance between the quinoline nitrogen and the Pt(111) surface increases slightly from 2.8 Å observed for the single AQ ligand to 3.2 Å.

The adsorption energy of a second AQ ligand in the most energetically favoured orientation is −1.34 eV. The attractive interaction of the 2AQ system lowers the energy by 0.12 eV compared to two infinitely separated AQ ligands. Ligand–ligand interactions are much weaker than the dominant ligand–surface interactions. Attractive interactions are due to the two intermolecular hydrogen bonds while repulsive interactions are attributed to unfavourable positioning on the surface as well as steric repulsion. The structure shown in Fig. 3b shows the 2 AQ ligands in a similar orientation to that shown in Fig. 3a but separated by approximately 6 Å. Although the structural properties of each ligand are similar to those of a single adsorbed AQ ligand shown in row a of Table 1, the separated co-adsorbed AQ ligands are slightly less energetically favoured than the co-adsorbed AQ ligands shown in Fig. 3a. The parallel configuration shown in Fig. 3c eliminates the possibility of forming intermolecular hydrogen bonds. In fact, this configuration shows repulsive ligand–ligand interactions and, as a result, its energy is 0.17 eV higher than that of the antiparallel configuration. Shorter ligand–ligand distances and the orientation of ligands with respect to each other are therefore crucial in forming attractive ligand–ligand interactions, such as hydrogen bonding. Strategies to increase the attractive interaction between adsorbed ligands include strengthening hydrogen bonds by using chlorinated or fluorinated compounds, increasing the number of possible hydrogen bonds and linking more complex ligands by covalent bonds.

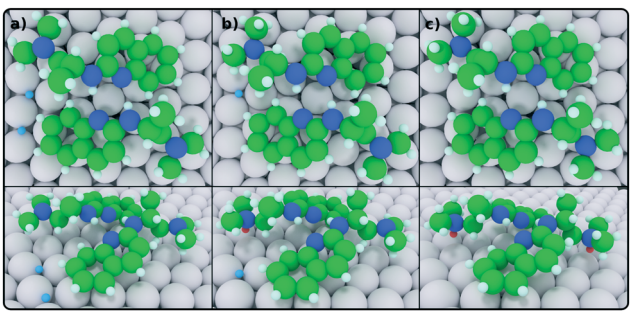

Fig. 4 The geometries of the three selected structures with zero, one and two hydrogens transferred to the ligand are shown. The corresponding energies are a) 0.00 eV, b) −0.38 eV, and c) −0.80 eV. Dissociated hydrogen atoms adsorbed on the Pt(111) surface are shown in light blue, and those transferred to the AQ ligand are shown in red.

3.3 Ligand protonation

The dissociative adsorption of molecular hydrogen is known to occur without any kinetic or thermodynamic barrier on Pt(111).[64] It is therefore possible for the AQ ligand (see Fig. 3a) to be protonated from readily available hydrogen atoms on the Pt(111) surface when the surface is exposed to H_2 gas. The adsorption energy of hydrogen on 2AQ-covered Pt(111) is −0.18 eV, which is slightly less exothermic than the experimental value (−0.3 eV) on bare Pt.[65] Both N^2 and N^3 atoms of the AQ ligand were considered for protonation. Both of these nitrogens are Lewis bases and, therefore, the most likely candidates for protonation. Our calculations show that protonating the N^3 atom, thus forming AQH as seen in Fig. S3a,† is thermodynamically favoured over protonating the N^2 atoms by 0.92 eV and the N^1 atom by 0.24 eV. The N^3 atom can adopt a tetrahedral configuration more easily because the methyl groups around it are a lesser steric hindrance compared to the quinoline moiety bonded to the N^2 atom.

The hydrogen transfer to the N^3 atom from the Pt(111) surface is exothermic by 0.38 eV and does not show any kinetic barrier (see Fig. 4). The N^3–Pt(111) distance decreases significantly from 3.8 Å to 3.2 Å as the N^3 atom adopts a tetrahedral configuration upon protonation. Protonating the second AQ ligand is exothermic by an additional 0.42 eV and results in both ligands having similar structural properties (see Fig. 4).

We employ the Bader charge method[62] to determine if a protonic hydrogen has been truly transferred to the ligand. On Pt(111), H atoms are approximately neutral with a partial charge of −0.1 e. After the transfer, the partial charge of the hydrogen atom is +0.4 e with an N–H distance of 1.07 Å, indicating the clear protonic nature, while the charge of the remaining surface hydrogen is still −0.1 e due to the interaction with the conducting metal surface. The outcome of this hydrogen transfer process is an asymmetrically charged hydrogen pair resembling the products of a heterolytic hydrogen dissociation. This result is significant because asymmetrically charged hydrogen pairs can influence the mechanism and energetics of reduction reactions.[66]

3.4 Levulinic acid reduction to 4-HPA on Pt(111)

In order to evaluate the effectiveness of the ligand-modified surface, we study the first step in the hydrogenation of LA, that is, the conversion of LA to 4-HPA. This reduction reaction can serve as a model for the hydrogenation of polyfunctional molecules and can help determine the effect of a ligand-modified Pt(111) surface on the reaction mechanism and energetics compared to that of a bare Pt(111) surface. Two different adsorption configurations for LA are considered: the first, LA1, has one internal hydrogen bond, while the second, LA2, does not (see Fig. S4†). Our calculations agree with a previous study[42] showing that gas-phase LA1 and LA2 are almost isoenergetic. LA1 is 0.05 eV less stable than LA2 (see I_1 and I_2 in Fig. 7 and Table 2) due to two

Table 2 Intermediates and transition states and their corresponding energies from the potential energy surface (Fig. 7). H** indicates the reacting hydrogen while * and (g) refer to adsorbed and gas-phase species. The figure column gives the reference to the figure that shows the atomic structure

Symbol	Intermediate structure/transition state	Energy (eV)	Fig.
I_1	LA1(g) + Pt(111) + H_2^*	0.05	NA
I_2	LA2(g) + Pt(111) + H_2^*	0.00	NA
I_3	LA1* + Pt(111) + H_2^*	−0.59	S4a†
I_4	LA2* + Pt(111) + H_2^*	−0.78	S4b†
I_5	Hydroxy LA1H* + Pt(111) + H_1^*	0.33	S5b†
I_6	Alkoxy LA1H* + Pt(111) + H_1^*	0.18	S6b and c†
I_7	Alkoxy LA2H* + Pt(111) + H_1^*	−0.03	S7b†
I_8	Hydroxy LA2H* + Pt(111) + H_1^*	−0.09	5b
I_9	4-HPA* + Pt(111)	−0.88	5c
I_{10}	LA2(g) + 2AQ* + Pt(111) + H_2^*	0.00	4a
I_{11}	LA2(g) + 2AQH* + Pt(111) + H_1^*	−0.38	4b
I_{12}	LA2* + 2AQH* + Pt(111) + H_1^*	−1.42	6a
I_{13}	Hydroxy LA2H* + 2AQ* + Pt(111) + H_1^*	−0.57	S9b†
I_{14}	4-HPA* + 2AQ* + Pt(111)	−1.25	6c
TS_1	Alkoxy LA1* + H_1^{**} + Pt(111) + H_1^*	0.62	S6a†
TS_2	Alkoxy LA2* + H_1^{**} + Pt(111) + H_1^*	0.56	S7a†
TS_3	Hydroxy LA1H* + Pt(111) + H_1^{**}	0.50	S5c†
TS_4	Alkoxy LA1H* + Pt(111) + H_1^{**}	0.36	S6d†
TS_5	Alkoxy LA2H* + Pt(111) + H_1^{**}	0.18	S7c†
TS_6	Hydroxy LA2H* + Pt(111) + H_1^{**}	−0.03	5b
TS_7	Simultan LA2* + 2AQ* + Pt(111) + H_2^{**}	−0.65	6b
TS_8	Hydroxy LA2H* + 2AQ*Pt(111) + H_1^{**}	−0.56	S9c†

competing effects. The formation of the internal hydrogen bond stabilizes the molecule while the non-planarity of the carbon skeleton destabilizes it. In contrast, whether in the gas phase or on the Pt(111) surface, LA2 lacks the internal hydrogen bond, but its carbon skeleton is nearly planar, as can be seen from the minimum energy structures in Fig. S4.† Nevertheless, both structures are kept to investigate LA reduction since the internal structure may influence the reaction mechanism.

The LA adsorption energies on a 2/9 ML H_2-covered Pt(111) surface are −0.59 eV for LA1 and −0.78 eV for LA2 (see I_3 and I_4 in Fig. 7 and Table 2). These adsorption energies are significantly less exothermic than the adsorption energy of −1.33 eV for LA on bare Ru(0001), which is also active for LA reduction.[42] Both LA conformers favour the parallel adsorption geometry on Pt(111) lying on average about 3.70 Å above the surface. For LA1, the carboxylic oxygen are located above Pt bridge sides, whereas for LA2, they are above hollow sites, as can be seen in Fig. 5a and S5a.† Similar to that of LA2 on Pt(111), the structure of LA adsorbed on Ru(0001) also lacks an internal hydrogen bond, but all of the oxygen atoms bind to surface bridge sites resulting in shorter distances between LA and the Ru(0001) surface.[42] We also considered the adsorption configurations with smaller LA–Pt distances similar to those identified on the Ru surface. Our calculations demonstrate, however, that these structures are unstable on Pt(111). During structural optimization, LA returns to a flat conformation with a larger LA–surface distance, similar to that shown in Fig. 5a.

Three possible reaction mechanisms are considered for the reduction of LA to 4-HPA: the hydroxy mechanism, the alkoxy mechanism, and the concerted mechanism. In the hydroxy mechanism, the H–O bond is initially formed, followed by C–H bond formation (light blue (LA1) and purple (LA2) paths in Fig. 7). These reaction steps are reversed in the alkoxy mechanism (green (LA1) and red (LA2) paths) and proceed simultaneously in the concerted mechanism. Although the concerted mechanism was considered, we were unable to locate a transition state as our NEB calculations always converted the concerted mechanism to either the hydroxy or the alkoxy mechanism. Fig. 7 and Table 2 display the relative potential energy surface for all stationary points along the examined reaction paths. The O–H bond formation in the hydroxy mechanism leads to metastable intermediates I_5 at +0.33 eV and I_8 at −0.09 eV for LA1 and LA2, respectively (see Fig. 7 and Table 2). Both intermediate structures resemble their respective initial adsorbed LA conformers. While no kinetic barriers are observed for the O–H bond formation, the thermodynamic barriers are +0.92 eV (LA1) and +0.69 eV (LA2) with respect to their initial states, I_3 and I_4. The C–H bond formation producing 4-HPA (I_9 in Fig. 7) is exothermic by 1.21 eV (LA1) and 0.79 eV (LA2) but has a small kinetic barrier of 0.17 eV and 0.06 eV, respectively. The hydrogen atom involved in the second hydrogenation step is relatively close to the surface with H–C distances of 2.03 Å for TS_3 (LA1) and 1.94 Å for TS_6 (LA2), as shown in Fig. S5† and 5. The overall reaction barrier, defined as the energy difference between the reactants and the highest energy

structure along the reaction path, is 1.09 eV for LA1 and 0.75 eV for LA2. The reaction energy for the hydrogenation of LA to 4-HPA adsorbed on Pt(111) is exothermic by −0.22 eV for LA1 and −0.10 eV for LA2. In comparison, the reduction of LA with no internal hydrogen bond on Ru(0001) must overcome a kinetic barrier of 1.36 eV to produce a hydroxy intermediate that is 0.88 eV higher in energy than the adsorbed LA reactant. The second hydrogenation on Ru(0001) is slightly exothermic (0.05 eV) with a kinetic barrier of 0.67 eV. The overall reaction barrier on Ru(0001) is 1.64 eV and the corresponding reaction energy for the hydrogenation to 4-HPA is endothermic by 0.82 eV.[42]

For the alkoxy mechanism, the key reaction steps are displayed in Fig. S6 (LA1) and S7† (LA2). The formation of intermediates I_6 for LA1 and I_7 for LA2 *via* hydrogen transfer to carbon is endothermic by 0.77 eV and 0.75 eV relative to their corresponding adsorbed LA configurations, I_3 and I_4, respectively (see Fig. 7). The energies for the transition states involved in this hydrogen transfer, TS_1 (LA1) and TS_2 (LA2), are 1.21 eV and 1.34 eV, respectively. The C–H distance is 1.45 Å for TS_1 and 1.44 Å for TS_2 as can be seen from Table S1.† The second hydrogen transfer is exothermic by 1.06 eV (LA1) and 0.85 eV (LA2) and has a small kinetic barrier of 0.18 eV and 0.21 eV corresponding to TS_4 and TS_5, respectively. The O–H distance is 1.55 Å for TS_4 and 1.47 Å for TS_5. On Ru (0001), a comparable alkoxy intermediate without an internal hydrogen bond is almost isoenergetic with its initial state, presenting activation energies of 0.67 eV and 1.29 eV for the first and the second hydrogenation, respectively.[42]

We observe that the hydrogenation of LA to 4-HPA follows different mechanisms on bare Pt(111) and on Ru(0001). The hydroxy mechanism is heavily preferred on Pt(111) while the alkoxy mechanism is favoured on Ru(0001). On Pt(111), the activation energy of the hydroxy mechanism is 0.59 eV lower than that of the alkoxy mechanism. In the case of Ru(0001), the activation energy for the alkoxy mechanism is 1.35 eV, while the activation energy for the hydroxy mechanism is 1.64 eV relative to the adsorbed reactants. Furthermore, the overall reaction is exothermic by −0.10 eV on Pt(111), while it is endothermic by 0.82 eV on Ru(0001). Previous experimental studies on the conversion of LA have suggested that 4-HPA is an intermediate, which loses a water molecule to form GVL.[45,67] We found that the 4-HPA conversion to GVL on Pt(111) is exothermic by −0.15 eV. No barriers have been computed, however, since the focus in the present work is to explore the effect of a ligand's presence compared to the bare surface rather than the full reaction network to GVL. Interestingly, previous DFT calculations suggest that GVL formation on Ru(0001) occurs *via* an alternative mechanism that does not involve 4-HPA.[42]

3.5 Levulinic acid reduction on 2AQH-modified Pt(111)

Lastly, we consider the effect of adsorbed AQ on LA hydrogenation, particularly in its protonated form, AQH. The adsorption energy of LA2 on 2AQH/Pt(111) (Fig. 4b) is −1.04 eV, slightly more exothermic than the adsorption on the bare Pt(111) surface (−0.78 eV). This indicates that the 2AQH ligands stabilize LA2, most likely due to hydrogen bonding between the N^3H and the LA2 oxygen (see Fig. S9a†). The average LA2–Pt(111) distance in the presence of 2AQH is 3.85 Å, which is 0.15 Å larger than that on the bare surface, again, most likely due to the interaction with the N^3H group.

The three possible mechanisms were also explored for the hydrogenation reaction of LA2 on ligand-modified Pt(111) (Fig. 6a). The major difference with the reduction of LA on the bare Pt(111) surface is that, as a result of the barrier-less exothermic AQ protonation, we consider a proton transfer from the AQ ligand to LA2. Our DFT results show that the concerted mechanism on 2AQH/Pt(111) is slightly endothermic by 0.17 eV and involves a transition state (TS_7) with an activation energy of 0.77 eV above the initial state, I_{12}, consisting of adsorbed LA2 and 2AQH (for a closer view of the transition state, see Fig. S8†). For the TS_7 structure, the O–H bond length is 1.40 Å, while the C–H bond length is 1.31 Å. This indicates the slightly asymmetric nature of the transition state because the O–H bond is only 69% formed while the C–H bond is already 84% formed. Our findings suggest that

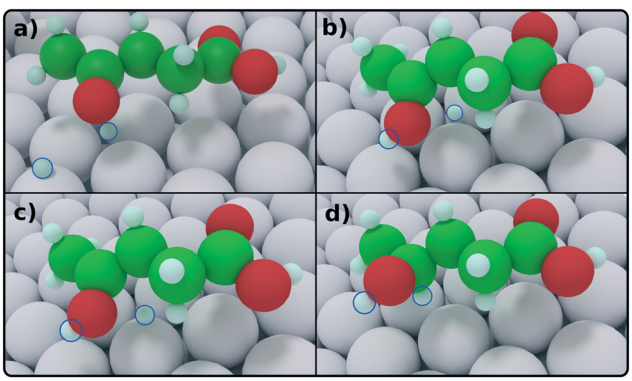

Fig. 5 Stationary points along the hydroxy mechanism for LA2 as referenced in Fig. 7 and Table 2: a) adsorbed reactants, I_4, b), intermediate I_8, c) transition state TS_6, and d) adsorbed 4-HPA, I_9. The hydrogen atoms involved in the reaction are circled for better visibility.

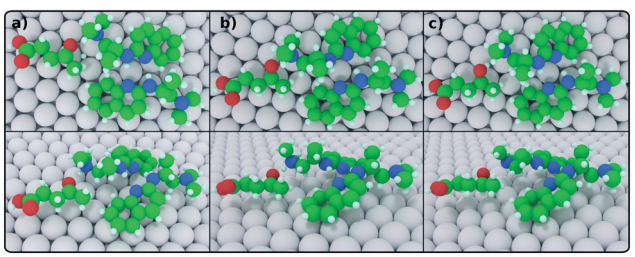

Fig. 6 Structures of the stationary states referenced in Fig. 7 for the concerted hydrogenation reaction of levulinic acid on a Pt(111) surface in the presence of 2AQH: a) adsorbed LA2 in the presence of 2AQ, (I_{12}), b) transition state (TS_7), and c) adsorbed 4-HPA (I_{14}).

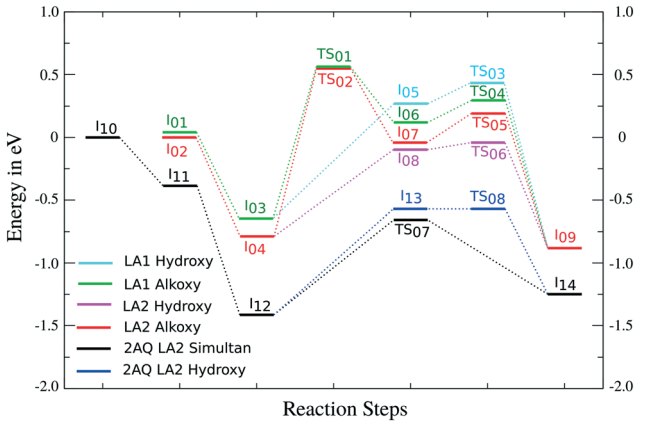

Fig. 7 Reaction network of LA to 4-HPA on the bare and 2AQ covered Pt(111) surfaces. The corresponding energies can be found in Table 2.

the proton at the N^3 atom is crucial for the concerted mechanism, as we were unable to locate the transition state for the simultaneous hydrogen transfer on the bare Pt(111) surface. In the hydroxy mechanism, the first hydrogen transfer, going from I_{12} to I_{13}, is endothermic by 0.85 eV (see Fig. 7 and S9†) with no additional kinetic barrier. The C–H bond formation in the hydroxy mechanism is exothermic by 0.69 eV. For this step, a transition state, TS_8, is observed; however, it is thermoneutral (+0.01 eV). The transition state C–H distance is 1.72 Å. This mechanism is very similar to the hydroxy mechanism observed on the bare surface except for a small barrier for the second hydrogen addition of 0.06 eV. The overall barrier for the hydroxy mechanism in the presence of 2AQ is 0.11 eV higher than that on the bare surface. We were unable to locate any transition states for the alkoxy mechanism; however, a thermodynamic barrier of 0.78 eV was determined by constraining the C–H distance to 1.08 Å, which is a typical distance for the computational method used. This intermediate is highly unstable and will revert back to its initial structure during the NEB calculation once the constraints are removed.

The hydroxy mechanism and the concerted mechanism are quite similar energetically, with an activation barrier relative to the I_{12} structure of 0.77 eV for the concerted mechanism and 0.85 eV for the hydroxy mechanism. The presence of 2AQ ligands on the Pt(111) surface changed the preferred reaction mechanism from the hydroxy mechanism to the concerted mechanism. The second AQ ligand could improve the enantioselectivity by sterically blocking the reaction sites. We note that under realistic reaction conditions many factors may influence levulinic acid hydrogenation and AQ ligand interaction with a metal catalyst including temperature, pressure, surface coverage, solvent effects, and surface structure, to just name but a few. By further improving the ligand design we believe it will be possible to positively influence the reactivity as well as enantioselectivity of this reaction.

4 Conclusions

We investigated the adsorption of AQ ligands on Pt(111), the interaction between adsorbed AQ ligands, AQ protonation, and the hydrogenation of LA to 4-HPA on the bare and AQ-modified Pt(111) surfaces using DFT. The exothermic adsorption of a single AQ ligand occurs when the quinoline ring aligns parallel over a Pt_4 rhombus. Two AQ ligands aligned antiparallel to each other form the most stable co-adsorption structure due to the weak ligand–ligand attraction from two intermolecular hydrogen bonds. In the presence of ligands, the transfer of dissociated hydrogen to the N^3 atom of the AQ ligand is a thermodynamically preferred non-activated process. Both LA configurations, with and without internal hydrogen bonding, bind exothermically to the Pt(111) surface. The AQ ligands also enhance LA binding to the Pt(111) surface. Three reaction mechanisms were considered for LA hydrogenation to 4-HPA on the bare Pt(111) and ligand-modified Pt(111) surfaces. On the bare Pt(111) surface, the hydroxy mechanism is energetically favoured over the alkoxy mechanism. The concerted mechanism is converted to either the hydroxy or alkoxy mechanisms on the bare Pt(111) surface. Our work demonstrates that adsorbed AQ can actively participate in catalytic reactions. By introducing AQ ligands onto the Pt(111) surface, the hydrogenation process changes dramatically. The protonated N^3 atom in AQ provides the protonic hydrogen to the ketone oxygen in LA, while the surface provides the other hydrogen atom to the carbonyl carbon thus forming 4-HPA. The concerted mechanism is favoured over the hydroxy mechanism by 0.1 eV. Overall, both bare and AQ-modified surfaces are equally active towards the conversion of LA to 4-HPA. Based on our computational findings, we believe that, with careful ligand design, it is possible to improve the activity as well as the selectivity of ligand-modified Pt catalysts for hydrogenation of polyfunctional molecules. These improved ligands could feature multiple sites that interact with the reactant to ensure selective positioning before and during the reaction as well as stronger ligand–ligand interactions. DFT calculations are a valuable tool in a systematic exploration of different ligand structures to establish trends for desirable ligand properties.

Conflicts of interest

There are no conflicts to declare.

Acknowledgements

The work was funded by the Academy of Finland Project 307623. We thank Prof. Petri Pihko for fruitful discussions and Dr Minttu Kauppinen and Dr Laura Laverdure for careful reading of the manuscript. The computational resources were provided by the Finnish Grid and Cloud Initiative as well as the CSC – IT Center for Science, Espoo, Finland (https://www.csc.fi/en/).

Notes and references

1 M. Tokunaga, J. Larrow, F. Kakiuchi and E. Jacobsen, *Science*, 1997, **277**, 936–938.
2 N. Maier, P. Franco and W. Lindner, *J. Chromatogr. A*, 2001, **906**, 3–33.
3 C. Hill and C. Prossermccartha, *Coord. Chem. Rev.*, 1995, **143**, 407–455.
4 M. Sawamura and Y. Ito, *Chem. Rev.*, 1992, **92**, 857–871.
5 H. Blaser, C. Malan, B. Pugin, F. Spindler, H. Steiner and M. Studer, *Adv. Synth. Catal.*, 2003, **345**, 103–151.
6 H. Blaser, B. Pugin and F. Spindler, *J. Mol. Catal. A: Chem.*, 2005, **231**, 1–20.
7 C. Li, X. Zhao, A. Wang, G. W. Huber and T. Zhang, *Chem. Rev.*, 2015, **115**, 11559–11624.
8 R. Noyori and S. Hashiguchi, *Acc. Chem. Res.*, 1997, **30**, 97–102.
9 T. Mallat, E. Orglmeister and A. Baiker, *Chem. Rev.*, 2007, **107**, 4863–4890.
10 J. Perez-Ramirez and N. Lopez, *Nat. Catal.*, 2019, **2**, 971–976.
11 A. Baiker, *Catal. Today*, 2005, **100**, 159–170.
12 C. Amiens, D. Ciuculescu-Pradines and K. Philippot, *Coord. Chem. Rev.*, 2016, **308**, 409–432.
13 P. Munnik, P. E. de Jongh and K. P. de Jong, *Chem. Rev.*, 2015, **115**, 6687–6718.
14 L. Zhang, M. Zhou, A. Wang and T. Zhang, *Chem. Rev.*, 2020, **120**, 683–733.
15 A. Bell, *Science*, 2003, **299**, 1688–1691.
16 V. Polshettiwar and R. S. Varma, *Green Chem.*, 2010, **12**, 743–754.
17 Y. Zhao, G. Fu and N. Zheng, *Catal. Today*, 2017, **279**, 36–44.
18 B. Wu and N. Zheng, *Nano Today*, 2013, **8**, 168–197.
19 M. A. Ortuno and N. Lopez, *Catal. Sci. Technol.*, 2019, **9**, 5173–5185.
20 D. Albani, Q. Li, G. Vile, S. Mitchell, N. Almora-Barrios, P. T. Witte, N. Lopez and J. Perez-Ramirez, *Green Chem.*, 2017, **19**, 2361–2370.
21 K. KaÅžmierczak, R. K. Ramamoorthy, A. Moisset, G. Viau, A. Viola, M. Giraud, J. Peron, L. Sicard, J.-Y. Piquemal, M. Besson, N. Perret and C. Michel, *Catal. Sci. Technol.*, 2020, **10**, 4923–4937.
22 Z. Cao, J. S. Derrick, J. Xu, R. Gao, M. Gong, E. M. Nichols, P. T. Smith, X. Liu, X. Wen, C. Coperet and C. J. Chang, *Angew. Chem., Int. Ed.*, 2018, **57**, 4981–4985.
23 M. Raynal, F. Portier, P. W. N. M. van Leeuwen and L. Bouteiller, *J. Am. Chem. Soc.*, 2013, **135**, 17687–17690.
24 I. Cano, A. M. Chapman, A. Urakawa and P. W. N. M. van Leeuwen, *J. Am. Chem. Soc.*, 2014, **136**, 2520–2528.
25 Y. Zhu, H. Qian, B. A. Drake and R. Jin, *Angew. Chem., Int. Ed.*, 2010, **49**, 1295–1298.
26 I. Schrader, S. Neumann, A. Sulce, F. Schmidt, V. Azov and S. Kunz, *ACS Catal.*, 2017, **7**, 3979–3987.
27 L. M. Martinez-Prieto, I. Cano, A. Marquez, E. A. Baquero, S. Tricard, L. Cusinato, I. del Rosal, R. Poteau, Y. Coppel, K. Philippot, B. Chaudret, J. Campora and P. W. N. M. van Leeuwen, *Chem. Sci.*, 2017, **8**, 2931–2941.
28 L. F. de L. e Freitas, B. Puertolas, J. Zhang, B. Wang, A. S. Hoffman, S. R. Bare, J. Perez-Ramirez, J. W. Medlin and E. Nikolla, *ACS Catal.*, 2020, **10**, 5202–5207.
29 G. Kumar, C.-H. Lien, M. J. Janik and J. W. Medlin, *ACS Catal.*, 2016, **6**, 5086–5094.
30 Z. Cao, J. S. Derrick, J. Xu, R. Gao, M. Gong, E. M. Nichols, P. T. Smith, X. Liu, X. Wen, C. Coperet and C. J. Chang, *Angew. Chem., Int. Ed.*, 2018, **57**, 4981–4985.
31 G. Vile, D. Baudouin, I. N. Remediakis, C. Coperet, N. Lopez and J. Perez-Ramirez, *ChemCatChem*, 2013, **5**, 3750–3759.
32 H.-U. Blaser and M. Studer, *Acc. Chem. Res.*, 2007, **40**, 1348–1356.
33 T. Burgi and A. Baiker, *Acc. Chem. Res.*, 2004, **37**, 909–917.
34 O. Sonderegger, G. Ho, T. Burgi and A. Baiker, *J. Mol. Catal. A: Chem.*, 2005, **229**, 19–24.
35 A. Baiker, *Chem. Soc. Rev.*, 2015, **44**, 7449–7464.
36 K. R. Hahn and A. Baiker, *J. Phys. Chem. C*, 2016, **120**, 20170–20180.
37 J. Q. Bond, D. M. Alonso, D. Wang, R. M. West and J. A. Dumesic, *Science*, 2010, **327**, 1110–1114.
38 D. W. Rackemann and W. O. S. Doherty, *Biofuel. Bioprod. Biorefin.*, 2011, **5**, 198–214.
39 L. Qi, Y. F. Mui, S. W. Lo, M. Y. Lui, G. R. Akien and I. T. Horvath, *ACS Catal.*, 2014, **4**, 1470–1477.
40 J.-P. Lange, R. Price, P. M. Ayoub, J. Louis, L. Petrus, L. Clarke and H. Gosselink, *Angew. Chem., Int. Ed.*, 2010, **49**, 4479–4483.
41 W. Luo, M. Sankar, A. M. Beale, Q. He, C. J. Kiely, P. C. A. Bruijnincx and B. M. Weckhuysen, *Nat. Commun.*, 2015, **6**, 6540.
42 O. Mamun, E. Walker, M. Faheem, J. Q. Bond and A. Heyden, *ACS Catal.*, 2017, **7**, 215–228.
43 H. Singh, N. Iyengar, R. Yadav, A. Rai and A. K. Sinha, *Sustainable Energy Fuels*, 2018, **2**, 1699–1706.
44 H. Gao and J. Chen, *J. Organomet. Chem.*, 2015, **797**, 165–170.
45 Y. Luo, J. Yi, D. Tong and C. Hu, *Green Chem.*, 2016, **18**, 848–857.
46 R. S. Assary and L. A. Curtiss, *Chem. Phys. Lett.*, 2012, **541**, 21–26.
47 O. Mamun, M. Saleheen, J. Q. Bond and A. Heyden, *J. Catal.*, 2019, **379**, 164–179.
48 F. M. A. Geilen, B. Engendahl, M. Hoelscher, J. Klankermayer and W. Leitner, *J. Am. Chem. Soc.*, 2011, **133**, 14349–14358.
49 Y. Kuwahara, H. Kango and H. Yamashita, *ACS Sustainable Chem. Eng.*, 2017, **5**, 1141–1152.
50 C. Michel, J. Zaffran, A. M. Ruppert, J. Matras-Michalska, M. Jedrzejczyk, J. Grams and P. Sautet, *Chem. Commun.*, 2014, **50**, 12450–12453.
51 L. E. Manzer, *Appl. Catal., A*, 2004, **272**, 249–256.
52 M. Nemanashi, J.-H. Noh and R. Meijboom, *Appl. Catal., A*, 2018, **550**, 77–89.
53 J. Mortensen, L. Hansen and K. Jacobsen, *Phys. Rev. B: Condens. Matter Mater. Phys.*, 2005, **71**, 035109.

54 J. Enkovaara, C. Rostgaard, J. J. Mortensen, J. Chen, M. Dułak, L. Ferrighi, J. Gavnholt, C. Glinsvad, V. Haikola, H. A. Hansen, H. H. Kristoffersen, M. Kuisma, A. H. Larsen, L. Lehtovaara, M. Ljungberg, O. Lopez-Acevedo, P. G. Moses, J. Ojanen, T. Olsen, V. Petzold, N. A. Romero, J. Stausholm-Møller, M. Strange, G. A. Tritsaris, M. Vanin, M. Walter, B. Hammer, H. HÃd'kkinen, G. K. H. Madsen, R. M. Nieminen, J. K. Nørskov, M. Puska, T. T. Rantala, J. Schiøtz, K. S. Thygesen and K. W. Jacobsen, *J. Phys.: Condens. Matter*, 2010, **22**, 253202.

55 A. H. Larsen, J. J. Mortensen, J. Blomqvist, I. E. Castelli, R. Christensen, M. Dulak, J. Friis, M. N. Groves, B. Hammer, C. Hargus, E. D. Hermes, P. C. Jennings, P. B. Jensen, J. Kermode, J. R. Kitchin, E. L. Kolsbjerg, J. Kubal, K. Kaasbjerg, S. Lysgaard, J. B. Maronsson, T. Maxson, T. Olsen, L. Pastewka, A. Peterson, C. Rostgaard, J. Schiotz, O. Schuett, M. Strange, K. S. Thygesen, T. Vegge, L. Vilhelmsen, M. Walter, Z. Zeng and K. W. Jacobsen, *J. Phys.: Condens. Matter*, 2017, **29**, 273002.

56 S. R. Bahn and K. W. Jacobsen, *Comput. Sci. Eng.*, 2002, **4**, 56–66.

57 J. Wellendorff, K. T. Lundgaard, A. Mogelhoj, V. Petzold, D. D. Landis, J. K. Norskov, T. Bligaard and K. W. Jacobsen, *Phys. Rev. B: Condens. Matter Mater. Phys.*, 2012, **85**, 235149.

58 A. H. Larsen, M. Vanin, J. J. Mortensen, K. S. Thygesen and K. W. Jacobsen, *Phys. Rev. B: Condens. Matter Mater. Phys.*, 2009, **80**, 195112.

59 G. Henkelman, B. Uberuaga and H. Jonsson, *J. Chem. Phys.*, 2000, **113**, 9901–9904.

60 G. Henkelman and H. Jonsson, *J. Chem. Phys.*, 2000, **113**, 9978–9985.

61 T. Frederiksen, M. Paulsson, M. Brandbyge and A.-P. Jauho, *Phys. Rev. B: Condens. Matter Mater. Phys.*, 2007, **75**, 205413.

62 G. Henkelman, A. Arnaldsson and H. Jonsson, *Comput. Mater. Sci.*, 2006, **36**, 354–360.

63 N. Bonalumi, A. Vargas, D. Ferri and A. Baiker, *Chem. – Eur. J.*, 2007, **13**, 9236–9244.

64 R. Olsen, G. Kroes and E. Baerends, *J. Chem. Phys.*, 1999, **111**, 11155–11163.

65 G. Yang, S. A. Akhade, X. Chen, Y. Liu, M.-S. Lee, V.-A. Glezakou, R. Rousseau and J. A. Lercher, *Angew. Chem., Int. Ed.*, 2019, **58**, 3527–3532.

66 S. Schauermann, *J. Phys. Chem. Lett.*, 2018, **9**, 5555–5566.

67 Y. Kuwahara, W. Kaburagi, Y. Osada, T. Fujitani and H. Yamashita, *Catal. Today*, 2017, **281**, 418–428.